Dalton Transactions

ROYAL SOCIETY OF CHEMISTRY

PAPER

View Article Online
View Journal | View Issue

Cite this: *Dalton Trans.*, 2020, **49**, 13685

The impact of metal coordination on the assembly of bis(indolyl)methane-naphthalene-diimide amphiphiles†

Sinan Bayindir, [a] Kwang Soo Lee, [b] Nurullah Saracoglu *[c] and Jon R. Parquette *[b]

Received 5th August 2020,
Accepted 22nd September 2020

DOI: 10.1039/d0dt02732d

rsc.li/dalton

The self-assembly and coordination of amphiphiles comprised of naphthalenediimide (NDI) and bis(indolyl)methane (BIM) chromophores were investigated as a function of pH and metal. As observed by TEM, SEM and AFM imaging, the self-assembly of NDI-BIM **1** produced irregular nanostructures at neutral pH in CH_3CN–H_2O (1 : 1); whereas, well-defined nanotubes were observed at pH 2. Conversely, Fmoc-protected, NDI-BIM **2** formed nanotubes at neutral pH and nonspecific aggregates at pH 2. Upon coordination of Cu^{2+} ions to the bis(indoyl)methane moiety, a reorganization from nanotubes to vesicular structures was observed.

Introduction

The development of reliable strategies to create multifunctional soft materials *via* the self-assembly of small molecules has enabled a wide range of applications in optoelectronics,[1,2] biomaterials,[3–5] sensing, and drug delivery,[6] *inter alia*.[7] The potential for these materials to display adaptivity, self-healing, and other forms of "intelligent" behavior would be enhanced by the capability to transition between multiple states.[8] Methods to dynamically modulate their structural features *via* external triggers are currently of tremendous interest.[9,10] Molecules, termed "molecular switches",[11,12] that interconvert between multiple configurational states upon irradiation[13] have the potential to induce changes in local monomer packing as a mechanism to modulate long-range nanostructural order. Although metal coordination has been exploited to drive the assembly of discrete self-assembled architectures,[14–16] and in the formation of coordination polymers,[17] there are fewer examples of coordination induced transformations among discrete self-assembled states.

Nanomaterials capable of coordinating metal ions in solution also have the potential to serve as chemosensors for metal analytes.[18–21] Additionally, bis(indolyl)methane compounds have found application as pharmaceuticals,[22,23] light-harvesting materials,[24,25] and as selective colorimetric/fluorimetric sensors for copper cations.[26–28] To create metal-binding nanostructure precursors, monomers **1** and **2** were comprised of bis(indolyl)methane (BIM), as the metal recognition site; 1,4,5,8-naphthalenetetracarboxylic acid diimide (NDI), to drive assembly by π–π interactions; and a charged L-lysine head group to impart amphiphilicity (Fig. 1). We reasoned that the amphiphilicity created by the juxtaposition of the NDI/BIM segments on one end with the polar lysine headgroup on the other would efficiently drive the assembly process in water.

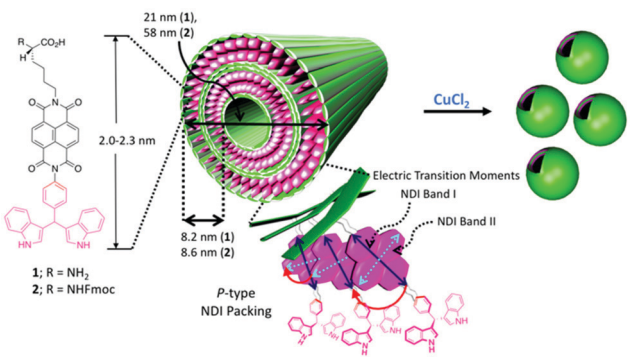

Fig. 1 Self-assembly of NDI-BIMs **1** and **2**. NDI-BIMs **1** and **2** assembled into nanotubes at pH 2 (for **1**) or pH 7 (for **2**), when the lysine head group was positively or negatively charged, respectively. Copper coordination to NDI-BIM **2** at pH 7 induced a transition from nanotubes to vesicular aggregates.

[a]*Department of Chemistry, Faculty of Sciences and Arts, Bingöl University, Bingöl, 12000, Turkey*
[b]*Department of Chemistry and Biochemistry, The Ohio State University, 100 W. 18th Ave., Columbus, Ohio 43210, USA. E-mail: parquett@chemistry.ohio-state.edu*
[c]*Department of Chemistry, Faculty of Sciences, Atatürk University, Erzurum, 25240, Turkey. E-mail: nsarac@atauni.edu.tr*

†Electronic supplementary information (ESI) available. See DOI: 10.1039/d0dt02732d

Results and discussion

The NDI-BIM amphiphiles, **1** and **2**, were prepared *via* the sequential monoimidation of NDI with (di(1*H*-indol-3-yl) methyl)aniline, **3**, followed by N^{α}-Boc-L-lysine or N^{α}-Fmoc-L-lysine to form **1**, after *N*-Boc deprotection, and **2**, respectively (Scheme 1). Alternatively, reversing the monoimidation sequence provided similar coupling efficiencies (Scheme S1†). Bis(indolyl)methane **3** was obtained *via* the $Bi(NO_3)_3{\cdot}5H_2O$-catalyzed reaction of indole with 4-nitrobenzaldehyde,[29] followed by reduction with $Ni(OAc)_2/NaBH_4$ or H_2/Pd–C (Scheme S1†).

We initially explored the self-assembly and metal-binding capability of NDI-BIM **1**, which displayed an unprotected lysine headgroup. Ultraviolet (UV-Vis) and circular dichroic (CD) spectra provided preliminary evidence for the self-assembly of **1** in CH_3CN–H_2O (1 : 1). NDI-BIM **1** exhibited absorbance bands corresponding to the NDI chromophore in the range of 240 nm (Band II) and 358/378 nm (Band I) in CH_3CN–H_2O at pH 7 (Fig. 2a). In pure 2,2,2-trifluoroethanol (TFE), in which **1** remained in the monomeric form, these bands occurred at 238 nm (Band II) and 356/376 nm. The red-shifting of the peaks going from TFE to CH_3CN–H_2O was consistent with the formation of a J-type aggregate.[30,31] Thus, intermolecular π–π interactions among the NDI units provided an additional driving force for the nanotube assembly process. Lowering the pH to 2 with trifluoroacetic acid (TFA) in CH_3CN–H_2O induced further bathochromic shifts to 360/381 nm (Band I), indicative of stronger π–π interactions. Similarly, whereas the CD spectrum of **1** in TFE was a flat line, Cotton effects in the range of 300–400 nm and 400–500 nm emerged in CH_3CN–H_2O (1 : 1, pH 2), corresponding to the NDI and BIM chromophores, respectively (Fig. 2b). Additionally, a strong positive excitonic couplet centered at *ca.* 240 nm, due to an NDI (Band II) transition, was present. The couplet at 240 nm emerged from transitions polarized along the short axis of the NDI, indicating the presence of a P-type intermolecular helical orientation (Fig. 1 and 2b).[32] At pH 7, the intensity of the CD peaks was significantly reduced, indicating a less efficient self-assembly process.

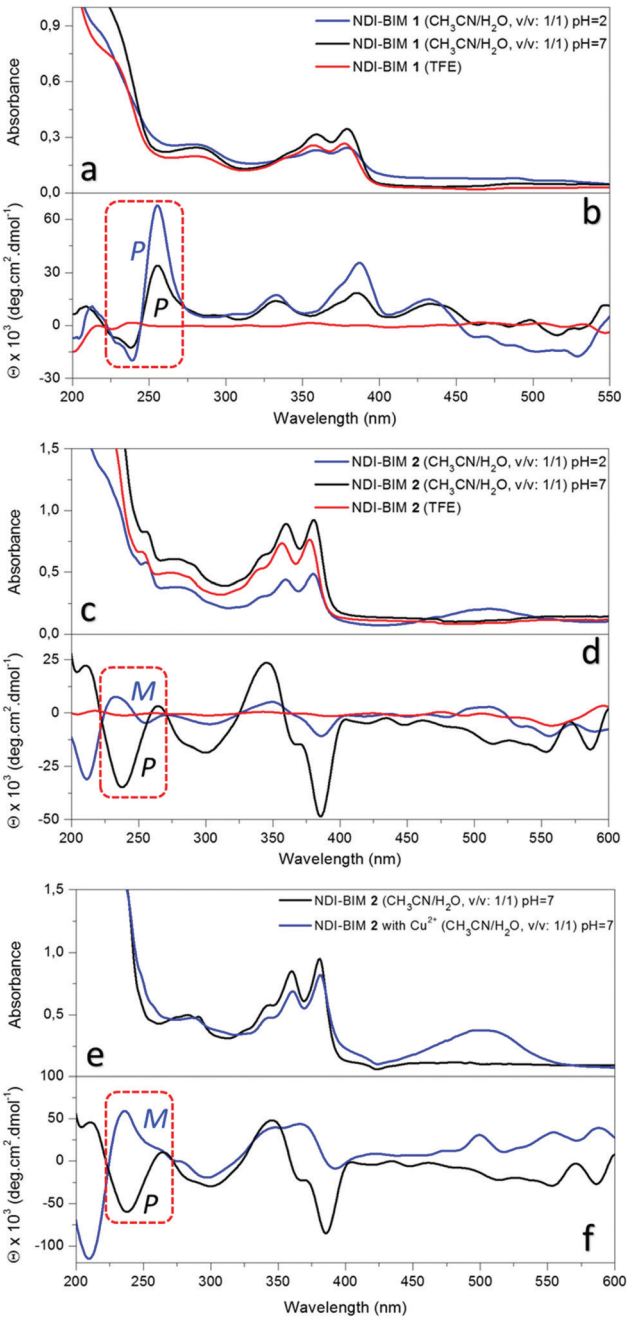

Fig. 2 UV and CD spectra of NDI-BIM **1** (a and b) and **2** (c and d) in CH_3CN–H_2O in and in pure TFE; and NDI-BIM **2-Cu** in CH_3CN–H_2O at pH 7 (e and f).

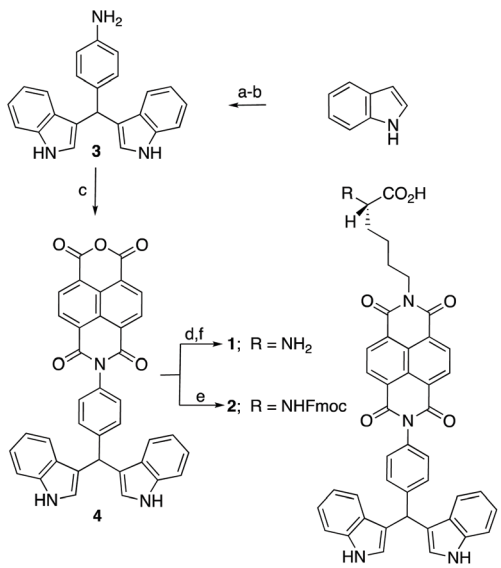

Scheme 1 (a) 4-Nitrobenzaldehyde, $Bi(NO_3)_3{\cdot}5H_2O$, CH_2Cl_2, 99%; (b) $NiCl_2{\cdot}6H_2O$, $NaBH_4$, CH_3OH, 98% or H_2, Pd–C, THF, 93%; (c) 1,4,5,8-naphthalenetetracarboxylic dianhydride, DMF, 100 °C, 98%; (d) N^{α}-(*t*-butoxycarbonyl)-L-lysine; DMF, 100 °C, 92%; (e) N^{α}-(((9*H*-fluoren-9-yl) methoxy)carbonyl)-L-lysine, DMF, 100 °C, 82%; (f) Et_3SiH, TFA, CH_2Cl_2, 85%.

Preliminary metal binding studies on NDI-BIM **1** with a wide range of metal chloride salts (Cr^{2+}, Co^{2+}, Cd^{2+}, Mg^{2+}, Sn^{2+}, Fe^{2+}, Cu^{2+}, Hg^{2+}, Mn^{2+}, Zn^{2+}) were performed by mixing a 1 : 1 ratio of the metal salts (10 mM) to NDI-BIM **1** (10 mM) in CH_3CN–H_2O (1 : 1) at pH 7. All of these metal salts failed to induce the appearance of absorption bands, expected in the range of ~500 nm, or any associated color changes, which would have been indicative of coordination to the BIM subunit.[26] The difficulty in metal complexation of **1** likely emerged from concomitant coordination of the free lysine headgroup in **1**.[33]

Accordingly, metal-binding studies were focused on NDI-BIM **2**, in which the lysine headgroup was protected as an N^{α}-Fmoc group. Although **2** was insoluble in pure water, the self-assembly could be evaluated in aqueous solvent mixtures (CH_3CN, TFE, TFE–H_2O (1 : 1), CH_3CN–H_2O (1 : 1)). Similar to **1**, amphiphile **2** exhibited red-shifting of the absorptions in the UV spectra going from TFE to CH_3CN; and from TFE to CH_3CN–H_2O (1 : 1, pH 7), indicative of J-type aggregation (Fig. S14†). The comparatively greater red-shifting in CH_3CN–H_2O (1 : 1, pH 7) confirmed that assembly was most efficient in this solvent mixture. In contrast to **1**, at pH 2, a transition emerged at 506 nm reflecting the partial protonation of the BIM chromophore under these conditions.[26] The CD spectrum showed cotton effects in the 300–350 and 350–400 nm ranges in CH_3CN–H_2O (1 : 1) at pH 2 and 7 (Fig. 2c). In contrast, significantly reduced CD signals in pure CH_3CN, and flat lines in TFE and TFE–H_2O (1 : 1) were indicative of a less efficient assembly process in these solvents, consistent with the UV studies. The excitonic couplet at ~240 nm, due to positive excitonic spitting of the NDI band II transition was apparent in the CD spectrum at pH 7, also indicative of P-type intermolecular π–π packing helicity of the NDI chromophores. Although the intensity of the couplet was substantially reduced, the sign was reversed at pH 2 (Fig. 2d). The lower overall intensity of the CD bands and the smaller excitonic couplet at ~240 nm suggested that the assembly process was inhibited at pH 2, producing partial aggregates with opposite M-type NDI helicity. This behavior contrasts with that of NDI-BIM **1**, which assembled more efficiently at pH 2 than at pH 7 (Fig. S5B†) into assemblies with P-type NDI helicity. Given the low basicity of the bis(indolyl)methane moiety present in **1** and **2**, the degree of protonation at pH 2 would be expected to be minimal.[34] Thus, the pH-dependent aggregation of the NDI-BIM monomers could be correlated with the charge state of the lysine headgroup. At low pH, amphiphile **1** displayed a positively charged headgroup, which enhanced the amphiphilicity of the monomer, thereby promoting aggregation. The charge would be much lower near the isoelectric pH at ~pH 7, thus impeding aggregation. In contrast, notwithstanding the small degree of BIM protonation, amphiphile **2** would remain neutral at pH 2 and negatively charged at pH 7, thereby facilitating aggregation at higher pH.

The capability of **2** to bind metal chloride salts was explored by mixing the metal salts (10 mM) and **2** (10 mM) in CH_3CN–H_2O (1 : 1) at pH 7 because these conditions promoted self-assembly and concomitantly minimized protonation of the BIM subunit. A scan of the potential of **2** to bind metal chloride salts (Cr^{2+}, Co^{2+}, Cd^{2+}, Mg^{2+}, Sn^{2+}, Fe^{2+}, Cu^{2+}, Hg^{2+}, Mn^{2+}, Zn^{2+}) revealed a high selectivity for Cu^{2+} (Fig. S1†).[26–28,35] In contrast to the other metal ions, the addition of $CuCl_2$ induced a color change from pale yellow to red, the appearance of absorption at 509 nm,[26] and slight red-shifting in the UV-Vis spectra, compared with uncomplexed **2**, from 359/380 nm to 360/381 nm (Fig. 2e). Similarly, the CD spectrum of NDI-BIM **2-Cu** showed cotton effects in the 300–400 nm range at pH 7 (Fig. 2f). However, whereas the excitonic couplet at ~240 nm, due to positive excitonic splitting of the NDI band II transition was present in the CD spectrum of NDI-BIM **2** at pH 7, the shape of the transitions in the 225–275 and 320–400 nm regions of the CD spectra were comparatively different for NDI-BIM **2-Cu**. In fact, the excitonic couplet at 240 nm resembled negative chirality, consistent with M-type NDI packing. These differences indicated a different intermolecular monomer packing orientation of **2-Cu** compared with uncomplexed **2**.

A 1 : 1 (**2** : Cu^{2+}) binding stoichiometry was determined from a plot of the absorption at 509 nm *versus* the **2**/$CuCl_2$ mole fraction (Job plot) (Fig. 3b, S4†).[36] The association constant (K_s) for the formation of **2-Cu** was determined to be 2.07 × 10^4 M^{-1} from the slope of a plot of $1/A - A_0$ *versus* $1/[Cu^{2+}]$ using the Benesi–Hildebrand equation (Fig. 3a and c).[37] The limits of detection and quantitation (LOD and LOQ) for Cu^{2+} ions were 22.1 μM and 66.9 μM in CH_3CN–H_2O (v/v: 1 : 1) solution (Fig. S3†), suggesting that **2** might find utility as a selective sensor of copper ions. The K_s and LOD values of **NDI-BIM 2** compared favorably to other published copper sensors (Table 1).[38–43]

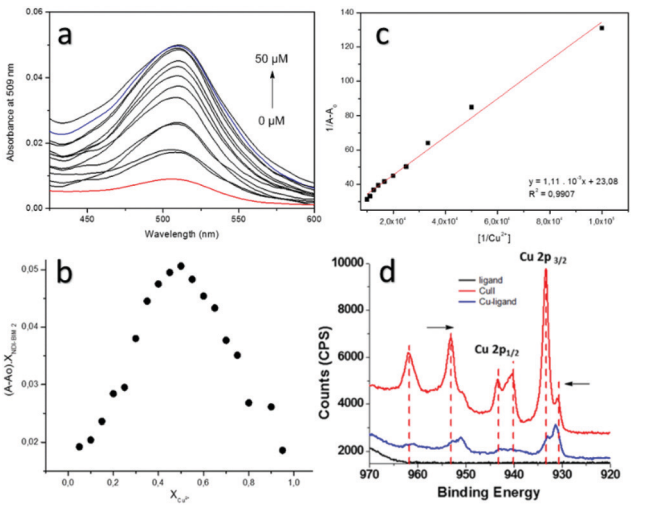

Fig. 3 (a) UV-vis titration of NDI-BIM **2** (10 mM) with $CuCl_2$ in CH_3CN–H_2O (1 : 1). (b) Job plot showing a 1 : 1 stoichiometry of complex NDI-BIM **2**-Cu. (c) Benesi–Hildebrand plot based on a 1 : 1 association stoichiometry between the NDI-BIM **2** with $CuCl_2$; (d) XPS Cu $2p_{1/2}$ and Cu $2p_{3/2}$ spectrum of NDI-BIM **2** (black), NDI-BIM **2** + $CuCl_2$ (blue) and $CuCl_2$ (red).

Table 1 Comparison of some Cu^{2+} selective chemosensors

Ref.	K_s (M^{-1})	LOD	Sensing ions
38	4.80×10^6 M^{-1}	10.1×10^{-6} M	Cu^{2+}
39	1.21×10^4 M^{-1}	2.31×10^{-6} M	Cu^{2+}, Hg^{2+}
40	3.26×10^4 M^{-1}	14.5×10^{-6} M	Cu^{2+}
41	2.08×10^4 M^{-1}	10.0×10^{-6} M	Cu^{2+}
42	3.10×10^6 M^{-1}	29.6×10^{-6} M	Cu^{2+}
43	3.80×10^6 M^{-1}	1.62×10^{-9} M	Cu^{2+}, S^{2-}
This work	2.07×10^4 M^{-1}	22.1×10^{-6} M	Cu^{2+}

The Cu 2p photoelectron and Cu LMM X-ray Auger electron spectra were consistent with copper in the divalent oxidation state (Fig. 3d).[44] Significant changes in the spectra were indicative of a change in the ligand environment around the copper. For example, a reversal in the relative intensities of the two peaks in the Cu $2p_{3/2}$ and Cu $2P_{1/2}$ spectral regions of **2-Cu**, compared with $CuCl_2$ were apparent.

The self-assembly of **1** and **2** was characterized by electron and atomic force microscopy (AFM). Accordingly, NDI-BIM **1** was incubated in CH_3CN–H_2O (1 : 1, 10 mM, 12 h) at pH 2 and 7. A sparse array of nanotubes, along with irregular aggregates, could be observed in the transmission electron microscopy (TEM) images of samples prepared at pH 7. In contrast, a homogeneous array of uniform nanotubes were observed at pH 2.0 (Fig. 4a and b, and S7†), consistent with the higher CD intensity at this pH. The nanotubes appeared as two white, parallel lines separated by a dark center, consistent with the cross-sectional view of a hollow, tubular structure. Similarly, imaging by scanning electron microscopy (SEM) revealed a protruding nanotube tip, confirming a tubular structure (Fig. 4c). The nanotubes displayed outer and inner diameters of 21.2 and 4.8 nm, respectively, and wall thicknesses of 8.2 nm, as imaged by TEM. Tapping-mode AFM imaging of the nanotubes on mica produced comparable cross-sectional heights (~15.8 nm) (Fig. 4d and S6†). Cross-sectional heights measured by AFM are typically slightly smaller than diameters determined by TEM, due to the compression of the nanotubes during imaging, often exhibiting heights of twice that of the wall thickness.[45]

Contrasting with the self-assembly of **1**, NDI-BIM **2** assembled into well-defined nanotubes after incubating at pH 7 (10 mM, 12 h) (Fig. 5a–d, and S8†), but formed a sparse array of vesicular aggregates at pH 2, consistent with the UV and CD spectra under those conditions. Similar to the nanotubes formed by **1**, SEM imaging revealed a nanotube end projecting out of the array, thereby confirming the nanotube morphology (Fig. 5c). Although the nanotubes exhibited larger diameters (58 nm), compared with those of **1** (pH 2), the wall thicknesses were similar (8.6 nm).

The large impact of headgroup charge on the efficacy of nanotube formation from **1** and **2** was consistent with an amphiphilic assembly process.[45–47] Thus, self-assembly was driven by sequestration of the hydrophobic NDI and BIM segments within the interior of the tube walls, while projecting the charged lysine headgroups on the inner and outer surfaces of the nanotubes. Additionally, the presence of J-aggregates, as evidenced by red-shifting the UV and the corresponding CD signals, indicated that intermolecular NDI π–π contacts played an important role in stabilizing the assembled nanotubes. The curvature of the membrane bilayers on the surface of the nanotubes likely emerges from the chirality and charge of the

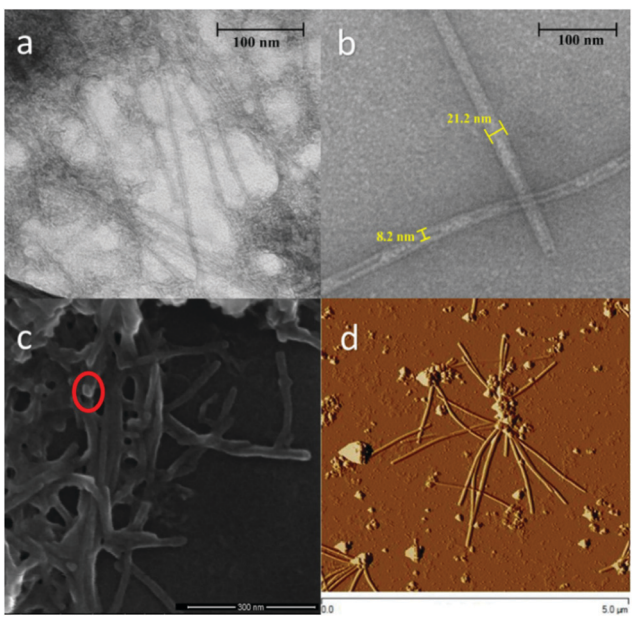

Fig. 4 (a) TEM image of NDI-BIM **1** at pH 7, (b) TEM image of NDI-BIM **1** at pH 2 (inset: nanotube dimensions), (c) SEM image of NDI-BIM **1** at pH 2 and (d) AFM image of NDI-BIM **1** at pH 2.

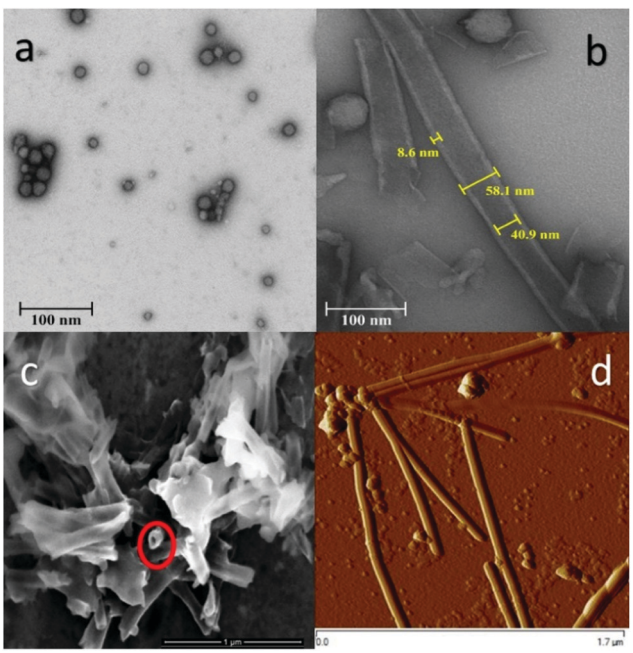

Fig. 5 (a) TEM image of NDI-BIM **2** at pH 2, (b) TEM image of NDI-BIM **2** at pH 7 (inset: nanotube dimensions), (c) SEM image of NDI-BIM **2** at pH 7 and (d) AFM image of NDI-BIM **2** at pH 7.

amphiphile headgroups, which causes the molecules to pack in tilted orientations.[48] Considering the extended lengths of **1** (2.0 nm) and **2** (2.3 nm) (Fig. 1 and S13†), the walls of the nanotubes from **1** (pH 2) and **2** (pH 7) would likely be comprised of two bilayers containing a total of four NDI-BIM molecules.

Following the addition of one equiv. of $CuCl_2$ to **2** (10 mM, CH_3CN–H_2O (1 : 1), pH 7), a structural transformation from a nanotube to a vesicle morphology was apparent by TEM, SEM and AFM imaging (Fig. 6a–c). The vesicles appeared as dark spheres with diameters ranging from 88–250 nm (Fig. S8†). Dynamic light scattering (DLS) also indicated a transition from large aggregates of 2000–8000 nm for **2** (10 mM, MeCN–H_2O, pH 7) to smaller aggregates (500–1400 nm) upon the addition of one equiv. $CuCl_2$ (Fig. 6d).

The change in morphology from nanotubes to vesicles likely emanated from an increase in the polarity of the BIM segment upon copper coordination, which modified the amphiphilic nature and structure of **2**. Access of the hydrophilic copper ions to the nonpolar interior wall segments of the nanotubes would be expected to be difficult.[6] However, self-assembled systems exist in dynamic equilibrium with the monomeric state, which often accounts for their stimuli responsivity and ability for self-repair.[49] Thus, the copper ions could be expected to bind NDI-BIM **2** *via* the monomer form, which drives the assembly process toward a vesicular morphology with M-type NDI packing.

In conclusion, we have designed and synthesized novel NDI-based amphiphiles containing a metal-binding BIM unit. These amphiphiles assembled into nanotubes most efficiently at pH 2 for **1** and pH 7 for **2**, when the lysine headgroup was positively or negatively charged, respectively. NDI-BIM **2** exhibited high selectivity for binding Cu^{2+}, as a 1 : 1 complex with an association constant of 2.07×10^4 M^{-1}. Copper coordination to **2** induced a transition from nanotubes to vesicular aggregates. The transition from nanotubes to vesicles likely emerged from a change in the amphiphilic nature of **2** upon copper binding. Low LOD and LOQ values indicated that **2** would be useful as a selective copper ion sensor.

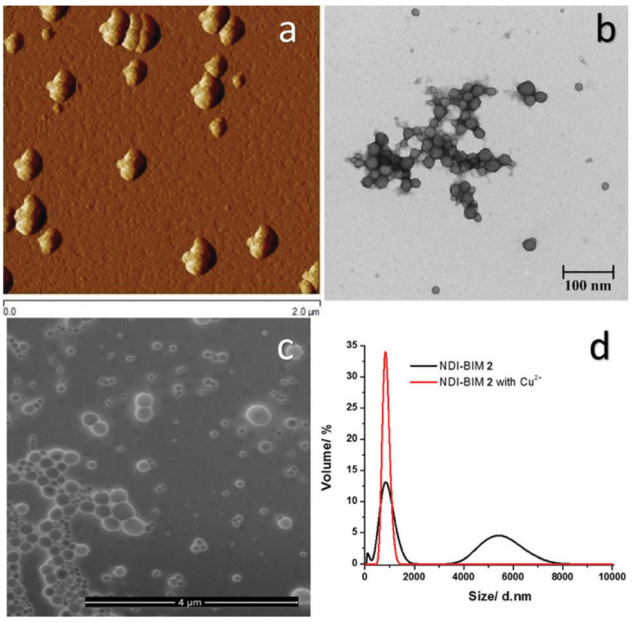

Fig. 6 (a) AFM, (b) TEM and (c) SEM images of NDI-BIM **2** (pH 7) after coordinating with Cu^{2+}; (d) DLS spectra of NDI-BIM **2** (black) and NDI-BIM **2-Cu** (red) in MeCN–H_2O (1 : 1, 10 mM, pH 7).

Experimental

General details

Circular dichroic (CD) spectra were taken with a JASCO CD spectrometer. Atomic force microscopy (AFM) was conducted in tapping mode under a nitrogen atmosphere. Transmission electron microscopy (TEM) was carried out with the Technai G2 Spirit instrument operating at 80 kV. Scanning Electron Microscopy (SEM) was carried out with the FEI Nova NanoSEM 400 scanning electron microscope. DLS measurements were performed using a Malvern Nano series Zetasizer. ^{1}H and ^{13}C NMR spectrums were recorded at 400 MHz on a Bruker Avance III instrument. ESI mass spectra were recorded on a Bruker MicroTOF coupled with HPLC in The Ohio-State University Chemical Instrument Center-Chemistry. All UV/Vis spectra were recorded with a SHIMADZU UV-2450 at 25 °C. All fluorescence spectroscopy was performed on a Shimadzu RF-6000 instrument using a cuvette with 1 mm or 1 cm pass length at 25 °C. Dimethylformamide (DMF) was dried by distillation from $MgSO_4$. Chromatographic separations were performed on silica gel 60 (230–400 mesh, 60 Å) using the indicated solvents. All reactions were performed under a nitrogen atmosphere.

4-(Di(1*H*-indol-3-yl)methyl)aniline (3)

To a suspension of 3,3′-((4-nitrophenyl)methylene)bis(1*H*-indole) (500 mg, 1.36 mmol) and $NiCl_2 \cdot 6H_2O$ (324 mg, 1.36 mmol) in CH_3OH (3.8 mL) was added $NaBH_4$ (257 mg, 6.80 mmol) at 0 °C and the mixture was stirred at 0 °C for 30 min. The reaction mixture was quenched by addition of sat. NH_4Cl at 0 °C and extracted with DCM. The combined organic layers were washed with brine (2 × 50 mL), and the organic phase was dried over anhydrous Na_2SO_4. The crude product (455 mg) was purified by flash chromatography with 10% EtOAc/hexane to give the product 4-(di(1*H*-indol-3-yl)methyl) aniline (**3**, 450.0 mg, 98%). ^{1}H-NMR (400 MHz, $CDCl_3$): δ 7.78 (s, NH, 2H), 7.42–7.40 (m, =CH, AA′ part of AA′BB′ system, 2H), 7.30 (d, J = 8.2 Hz, =CH, 2H), 7.16 (t, J = 7.7 Hz, =CH, 2H), 7.12–7.10 (m, =CH, BB′ part of AA′BB′ system, 2H), 7.01 (t, J = 7.7 Hz, =CH, 2H), 6.61–6.58 (m, =CH, 4H), 5.78 (s, CH, 1H), 3.52 (bs, NH_2, 2H); ^{13}C-NMR (100 MHz, $CDCl_3$): δ 144.3, 136.7, 134.4, 129.5, 127.1, 123.6, 121.8, 120.2, 120.1, 119.3, 115.2, 111.1, 39.3; IR (KBr, cm^{-1}): 3456, 3423, 3051, 2980, 2394, 1593, 1510, 1458, 1337, 916; ESI-MS calc. for $C_{23}H_{19}N_3$: $[M + H]^+$: 338.1657, found: 338.1652; TLC: R_f = 0.61 (EtOAc/hexane (10%), 254 nm).

3,3′-Bis(indolyl)methane-NDI monoimide (4)

1,4,5,8-Naphthalenetetracarboxylic dianhydride (**NDI**, 397 mg, 1.48 mmol) was dissolved in DMF (15 mL) and solution of 4-(di(1*H*-indol-3-yl)methyl)aniline (**3**, 500 mg, 1.48 mmol) in DMF (5 mL) was added slowly *via* dropping funnel at 90 °C. The reaction mixture was degassed with a nitrogen stream and heated to 100 °C. After 4 h, the solvent was removed by evaporation at reduced pressure, and the residue was purified by flash chromatography with 10% DCM–MeOH to give 3,3′-bis(indolyl)methane-NDI monoimide (BIM-NDI, 857 mg, 98%, m.p. > 400 °C (DCM)) as eluent affording a red solid. ^{1}H-NMR (400 MHz, DMSO-d_6): δ 10.88 (s, NH, 2H), 8.73–8.71 (m, =CH, AA′ part of AA′BB′ system, 2H), 8.67–8.65 (m, =CH, BB′ part of AA′BB′ system, 2H), 7.54–7.52 (m, =CH, AA′ part of AA′BB′ system, 2H), 7.38–7.31 (m, =CH, 6H), 7.06 (t, J = 7.9 Hz, =CH, 2H), 6.93 (d, J = 2.2 Hz, =CH, 2H), 6.89 (d, J = 7.9 Hz, =CH, 2H), 5.95 (s, CH, 1H); ^{13}C-NMR (100 MHz, DMSO-d_6): δ 162.9, 162.6, 159.8, 145.3, 136.6, 133.0, 131.8, 130.3, 128.6, 128.5, 127.7, 126.6, 126.5, 123.7, 123.6, 120.9, 119.1, 118.2, 117.8, 111.5, 35.7; IR (KBr, cm^{-1}): 3360, 3048, 3030, 3011, 2933, 2866, 2637, 2400, 2394, 1907, 1788, 1600, 1526, 1592, 1340, 1285, 1130, 827; ESI-MS calc. for $C_{37}H_{21}N_3O_5$: $[M]^+$: 587.1461, found: 587.1441; TLC: R_f = 0.26 (DCM/MeOH (10%), 254 nm).

N^{α}-Boc-L-lysine-NDI-3,3′-bis(indolyl)methane

The 3,3′-bis(indolyl)methane-NDI monoimide **4** (500 mg, 0.85 mmol) was dissolved in DMF (10 mL). After a solution of N^{α}-(*tert*-butoxycarbonyl)-L-lysine (209 mg, 0.85 mmol) was added in DMF (5 mL), the reaction was degassed with a nitrogen stream and heated to 100 °C for 3 h. DMF was removed by evaporation at reduced pressure, and the residue was purified by flash chromatography with 10% DCM–MeOH to give N^{α}-Boc-L-lysine-NDI-3,3′-bis(indolyl)methane (637 mg, 92%, m.p. > 400 °C (DCM)) as eluent affording red solid. ^{1}H-NMR (400 MHz, DMSO-d_6): δ 11.50 (bs, CO_2H, 1H), 10.89 (bs, NH, 2H), 8.63–8.60 (m, =CH, AA′ part of AA′BB′ system, 2H), 8.59–8.57 (m, =CH, BB′ part of AA′BB′ system, 2H), 7.56–7.54 (m, =CH, AA′ part of AA′BB′ system, 2H), 7.39–7.33 (m, =CH, 6H), 7.06 (t, J = 8.1 Hz, =CH, 2H), 6.95 (bs, =CH, 2H), 6.91 (t, J = 6.0 Hz, =CH, 2H), 5.97 (s, CH, 1H), 5.25 (d, J = 4.0 Hz, NH, 1H), 4.03 (bs, CH_2, 2H), 3.89–3.88 (m, CH_2, 1H), 1.68–1.65 (m, CH_2, 4H), 1.42–1.39 (m, CH_2, 2H), 1.36 (s, CH_3, 9H); ^{13}C-NMR (100 MHz, DMSO-d_6): δ 174.2, 162.7, 162.4, 155.6, 145.3, 136.6, 130.4, 130.3, 128.7, 128.5, 126.7, 126.6, 126.3, 126.1, 126.0, 123.6, 120.9, 119.1, 118.2, 117.8, 111.5, 77.9, 53.3, 35.7, 30.7, 30.5, 28.2, 27.0, 23.2; IR (cm^{-1}): 3366, 3048, 3011, 2945, 2859, 2637, 2400, 1890, 1526, 1907, 1591, 1542, 1441, 1285, 1130, 827; ESI-MS calc. for $C_{48}H_{41}N_5O_8$:[M]: 815.2955, found: 815.2947; TLC: R_f = 0.21 (DCM/MeOH (15%), 254 nm).

NH_2-L-lysine-NDI-3,3′-bis(indolyl)methane (1)

To the solution of N^{α}-Boc-L-lysine-NDI-3,3′-bisindole (500.0 mg, 0.62 mmol) in TFA/DCM (1 : 1, 10 mL) was added 1 mL of triethylsilane. The mixture was stirred for 2 h at room temperature before the solvent was removed by evaporation at reduced pressure affording a dark red oil. The crude oil was washed with cold diethyl ether (3 × 15 mL) and MeCN (1 × 15 mL) resulting a dark red precipitate and crude product was dissolved in H_2O : MeCN (1 : 1, 40 mL). The crude product (390 mg) was purified by reversed phase HPLC on preparative Varian Dynamax C18 column eluting with a linear gradient of MeCN/H_2O with 0.1% TFA (20/80 to 90/10 over 5 h). As a result of this purification, H_2N-L-lysine-NDI-3,3′-bis(indolyl)methane was obtained (**1**, 372 mg, 85%, m.p. > 400 °C (DCM)) as a dark red solid. ^{1}H-NMR (400 MHz, DMSO-d_6): δ 10.93 (s, =NH, 2H), 8.65–8.63 (m, =CH, 4H), 7.47–7.45 (m, =CH, AA′ part of AA′BB′ system, 2H), 7.36 (d, J = 8.2 Hz, =CH, 2H), 7.32 (d, J = 8.2 Hz, =CH, 2H), 7.32–7.25 (m, =CH, 4H), 7.07 (t, J = 8.2 Hz, =CH, 2H), 7.05–6.97 (m, =CH, 3H), 6.16 (s, CH, 1H), 4.07–4.05 (m, CH_2, 2H), 3.93 (bs, CH, 1H), 1.86–1.83 (m, CH_2, 2H), 1.71–1.70 (m, CH_2, 2H) 1.47 (bs, NH_2, 2H), 1.43–1.40 (m, CH_2, 2H); ^{13}C-NMR (100 MHz, DMSO-d_6): δ 171.0, 162.8, 162.6, 162.5, 142.3, 136.4, 133.0, 130.4, 128.8, 127.0, 126.8, 126.4, 126.2, 123.3, 121.0, 118.7, 118.5, 118.3, 113.4, 111.4, 100.9, 51.8, 37.7, 30.6, 29.7, 27.0, 21.9; IR (cm^{-1}): 3360, 3050, 3015, 2940, 2859, 2400, 1907, 1597, 1546, 1445, 1285, 1238, 1198, 1130, 1051, 930, 827; ESI-MS calc. for $C_{43}H_{33}N_5O_6$: $[M + H]^+$:716.2509, found: 716.2554.

N^{α}-Fmoc-L-lysine-NDI-bis(indolyl)methane (2)

The 3,3′-bis(indolyl)methane-NDI-monoimide (**4**, 500 mg, 0.85 mmol) was dissolved in DMF (10 mL). After a solution of N^{α}-Fmoc-L-Lys-OH (314 mg, 0.85 mmol) in DMF (5 mL) was added, the reaction was degassed with a nitrogen stream and heated to 100 °C for 4 h. DMF was removed by evaporation at reduced pressure. The crude product (720 mg) was purified by reversed phase HPLC on preparative Varian Dynamax C18 column eluting with a linear gradient of MeCN/H_2O with 0.1% TFA (20/80 to 90/10 over 7 h). As a result of this purification, N^{α}-Fmoc-L-lysine-NDI-3,3′-bis(indolyl)methane (**2**, 655 mg, 82%, m.p. > 400 °C (DCM)) was obtained affording a red solid. ^{1}H-NMR (400 MHz, DMSO-d_6): δ 10.92 (s, NH, 2H), 8.63–8.59 (m, =CH, 4H, 8.63–8.59 (m, =CH, 4H), 8.54–8.50 (m, =CH, AA′ part of AA′BB′ system, 2H), 8.33 (d, J = 7.5 Hz, =CH, 2H), 8.02 (d, J = 7.5 Hz, =CH, 2H), 7.55 (d, J = 8.0 Hz, =CH, 2H), 7.45–7.40 (m, =CH, 8H), 7.05 (d, J = 8.0 Hz, =CH, 2H), 6.96–6.92 (m, =CH, 4H), 5.97 (bs, CH, 1H), 5.49 (bs, NH, 1H), 4.31–4.20 (m, CH, 1H), 4.08–3.93 (m, CH, CH_2, 3H), 3.40 (dd, J = 16.5, 8.8 Hz, CH_2, 2H), 1.82–1.56 (m, CH_2, 4H), 1.31–1.16 (m, CH_2, 2H); ^{13}C-NMR (100 MHz, DMSO-d_6): δ 185.5, 162.7, 162.4, 145.3, 137.3, 136.6, 133.0, 132.9, 130.3, 128.8, 128.6, 127.2, 127.1, 126.6, 126.0, 125.6, 124.7, 123.6, 122.4, 121.7, 121.3, 120.9, 119.9, 119.1, 118.2, 117.9, 111.5, 109.6, 56.6, 40.1, 36.9, 35.7, 30.7, 28.8, 23.6, 15.2; IR (cm^{-1}): 3455, 3366, 3165, 3059, 3048, 3011, 2945, 2859, 2637, 2400, 1890, 1526, 1907, 1591, 1542, 1441, 1285, 1130, 827; ESI-MS calc. for $C_{58}H_{43}N_5O_8$: $[M + Na]^+$: 960.3009, found: 960.3032.

UV-Vis detection of cations

A solution of NDI-BIM **2** (1×10^{-2} M) and cations (chloride of metal ions, 1×10^{-2} M) were prepared in CH_3CN/H_2O (1 : 1/

v : v). The solution (1×10^{-5} M) was then placed in a quartz cell and the UV-Vis spectrum was recorded. After the introduction of the solution of cations (1 equiv.), the changes in absorbance intensity were recorded at room temperature each time (Fig. S1†).

UV-Vis titration of the ligand with $CuCl_2$

The solution of NDI-BIM **2** (1×10^{-2} M) and $CuCl_2$ (1×10^{-2} M) was prepared in CH_3CN–H_2O (1 : 1/v : v) at pH 7. The concentration of a solution of ligand used in the experiments was 1×10^{-5} M. The UV-Vis titration spectra were recorded by adding a corresponding concentration of $CuCl_2$ to the solution of a ligand in CH_3CN–H_2O (v/v: 1 : 1). Each titration was repeated at least twice until consistent values were obtained (Fig. S2†).

Job's plot measurement

NDI-BIM **2** was dissolved in CH_3CN–H_2O (1 : 1/v : v) to achieve a concentration of 1×10^{-2} M. 5.00, 4.75, 4.50, 4.25, 4.00, 3.75, 3.50, 3.25, 3.00, 2.75, 2.50, 2.25, 2.00, 1.75, 1.50, 1.25, 1.00, 0.75, 0.50 and 0.25 mL aliquots of the ligand solution were taken and transferred to vials. $CuCl_2$ was dissolved in CH_3CN–H_2O (1 : 1/v : v) to make solution concentrations of 1×10^{-2} M. 0.25, 0.50, 0.75, 1.00, 1.25, 1.50, 1.75, 2.00, 2.25, 2.50, 2.75, 3.00, 3.25, 3.50, 3.75, 4.00, 4.25, 4.50, 4.75 and 5 mL aliquots of the copper solution were then added to each ligand solution. Each vial had a total volume of 5 mL. After shaking the vials for a few seconds, UV–vis spectra were taken at room temperature (Fig. S4†).

Conflicts of interest

There are no conflicts of interest to declare.

Acknowledgements

This manuscript is based upon work supported by the National Science Foundation (CHE-1708390) and by the U.S. Army Research Laboratory and the U.S. Army Research Office under grant number W911NF-14-1-0305. S. Bayindir is thankful for the doctoral fellowship (2214/A) to the Scientific and Technological Research Council of Turkey (TÜBİTAK). N. Saracoglu is grateful for the supports to the Council of Higher Education (CoHE) of Turkey and Atatürk University. We acknowledge the technical assistance and usage of the Campus Microscopy & Imaging Facility at OSU.

References

1 T. E. Kaiser, H. Wang, V. Stepanenko and F. Wurthner, *Angew. Chem., Int. Ed.*, 2007, **46**, 5541–5544.
2 M. Gao, S. Paul, C. D. Schwieters, Z.-Q. You, H. Shao, J. M. Herbert, J. R. Parquette and C. P. Jaroniec, *J. Phys. Chem. C*, 2015, **119**, 13948–13956.
3 H. G. Cui, M. J. Webber and S. I. Stupp, *Biopolymers*, 2010, **94**, 1–18.
4 T. Dvir, B. P. Timko, D. S. Kohane and R. Langer, *Nat. Nanotechnol.*, 2011, **6**, 13–22.
5 S. G. Zhang, *Nat. Biotechnol.*, 2003, **21**, 1171–1178.
6 S. H. Kim, J. A. Kaplan, Y. Sun, A. Shieh, H. L. Sun, C. M. Croce, M. W. Grinstaff and J. R. Parquette, *Chem. – Eur. J.*, 2015, **21**, 101–105.
7 K. Thorkelsson, P. Bai and T. Xu, *Nano Today*, 2015, **10**, 48–66.
8 I. Tomatsu, K. Peng and A. Kros, *Adv. Drug Delivery Rev.*, 2011, **63**, 1257–1266.
9 B. A. Grzybowski, C. E. Wilmer, J. Kim, K. P. Browne and K. J. M. Bishop, *Soft Matter*, 2009, **5**, 1110–1128.
10 T. Fenske, H. G. Korth, A. Mohr and C. Schmuck, *Chem. – Eur. J.*, 2012, **18**, 738–755.
11 B. L. Feringa, *J. Org. Chem.*, 2007, **72**, 6635–6652.
12 G. Vives and J. M. Tour, *Acc. Chem. Res.*, 2009, **42**, 473–487.
13 M. Natali and S. Giordani, *Chem. Soc. Rev.*, 2012, **41**, 4010–4029.
14 J. Li, X. Li, F. Jiang, X. Li, X. Xie, L. Wu, L. Wang, M. Lee and W. Li, *Chem. – Eur. J.*, 2017, **23**, 13510–13517.
15 M. Dukh, D. Šaman, J. Kroulík, I. Černý, V. Pouzar, V. Král and P. Drašar, *Tetrahedron*, 2003, **59**, 4069–4076.
16 W. Wang, Y. X. Wang and H. B. Yang, *Chem. Soc. Rev.*, 2016, **45**, 2656–2693.
17 W. Li, Y. Kim, J. Li and M. Lee, *Soft Matter*, 2014, **10**, 5231–5242.
18 M. Ahmed, M. Faisal, A. Ihsan and M. M. Naseer, *Analyst*, 2019, **144**, 2480–2497.
19 N. Kwon, Y. Hu and J. Yoon, *ACS Omega*, 2018, **3**, 13731–13751.
20 T. A. Fayed, M. N. El-Nahass, H. A. El-Daly and A. A. Shokry, *Appl. Organomet. Chem.*, 2019, **33**, e4868.
21 J. Zhang, F. Cheng, J. Li, J. J. Zhu and Y. Lu, *Nano Today*, 2016, **11**, 309–329.
22 M. Damodiran, D. Muralidharan and P. T. Perumal, *Bioorg. Med. Chem. Lett.*, 2009, **19**, 3611–3614.
23 A. Kamal, M. N. A. Khan, K. S. Reddy, Y. V. V. Srikanth, S. K. Ahmed, K. P. Kumar and U. S. Murthy, *J. Enzyme Inhib. Med. Chem.*, 2009, **24**, 559–565.
24 M. Kirkus, M. H. Tsai, J. V. Grazulevicius, C. C. Wu, L. C. Chi and K. T. Wong, *Synth. Met.*, 2009, **159**, 729–734.
25 S. Sathiyaraj, K. A. Kumar, A. K. J. Shanavas and A. S. S. Nasar, *ChemistrySelect*, 2017, **2**, 7108–7116.
26 A. K. Mahapatra, G. Hazra, N. K. Das and S. Goswami, *Sens. Actuators, B*, 2011, **156**, 456–462.
27 X. He, S. Hu, K. Liu, Y. Guo, J. Xu and S. Shao, *Org. Lett.*, 2006, **8**, 333–336.
28 R. Martínez, A. Espinosa, A. Tárraga and P. Molina, *Tetrahedron*, 2008, **64**, 2184–2191.
29 S. Bayindir and N. Saracoglu, *RSC Adv.*, 2016, **6**, 72959–72967.
30 A. P. H. J. Schenning, P. Jonkheijm, E. Peeters and E. W. Meijer, *J. Am. Chem. Soc.*, 2001, **123**, 409.
31 F. Würthner, *Chem. Commun.*, 2004, **35**, 1564–1579.

32 J. Gawronski, M. Brzostowska, K. Kacprzak, H. Kolbon and P. Skowronek, *Chirality*, 2000, **12**, 263–268.
33 S. Wiejak, E. Masiukiewicz and B. Rzeszotarska, *Chem. Pharm. Bull.*, 1999, **47**, 1489–1490.
34 R. L. Hinman and J. Lang, *J. Am. Chem. Soc.*, 1964, **86**, 3796–3806.
35 R. M. N. Kalla, S. C. Hong and I. Kim, *ACS Omega*, 2018, **3**, 2242–2253.
36 P. Thordarson, *Chem. Soc. Rev.*, 2011, **40**, 1305–1323.
37 T. M. Elmorsi, T. S. Aysha, O. Machalický, M. B. I. Mohamed and A. H. Bedair, *Sens. Actuators, B*, 2017, **253**, 437–450.
38 S. Ghosh, A. Ganguly, M. R. Uddin, S. Mandal, M. A. Alam and N. Guchhait, *Dalton Trans.*, 2016, **45**, 11042–11051.
39 S. Bayindir, *J. Photochem. Photobiol., A*, 2019, **372**, 235–244.
40 S. Bayindir and M. Toprak, *Spectrochim. Acta, Part A*, 2019, **213**, 6–11.
41 Y. Zhao, X.-B. Zhang, Z.-X. Han, L. Qiao, C.-Y. Li, L.-X. Jian, G.-L. Shen and R.-Q. Yu, *Anal. Chem.*, 2009, **81**, 7022–7030.
42 D. Bansal and R. Gupta, *Dalton Trans.*, 2016, **45**, 502–507.
43 A. Paul, S. Anbu, G. Sharma, M. L. Kuznetsov, M. F. í. C. Guedes da Silva, B. Koch and A. J. L. Pombeiro, *Dalton Trans.*, 2015, **44**, 16953–16964.
44 S. Shuvaev, I. S. Bushmarinov, I. Sinev, A. O. Dmitrienko, K. A. Lyssenko, V. Baulin, W. Grünert, A. Y. Tsivadze and N. Kuzmina, *Eur. J. Inorg. Chem.*, 2013, **2013**, 4823–4831.
45 S. Vauthey, S. Santoso, H. Y. Gong, N. Watson and S. G. Zhang, *Proc. Natl. Acad. Sci. U. S. A.*, 2002, **99**, 5355–5360.
46 H. Shao, J. Seifert, N. C. Romano, M. Gao, J. J. Helmus, C. P. Jaroniec, D. A. Modarelli and J. R. Parquette, *Angew. Chem., Int. Ed.*, 2010, **49**, 7688–7691.
47 S. Y. Tu, S. H. Kim, J. Joseph, D. A. Modarelli and J. R. Parquette, *J. Am. Chem. Soc.*, 2011, **133**, 19125–19130.
48 J. V. Selinger, M. S. Spector and J. M. Schnur, *J. Phys. Chem. B*, 2001, **105**, 7157–7169.
49 T. Aida, E. W. Meijer and S. I. Stupp, *Science*, 2012, **335**, 813.